INTERNATIONAL JOURNAL FOR NUMERICAL METHODS IN FLUIDS
Int. J. Numer. Meth. Fluids 2008; **56**:2139–2150
Published online 19 September 2007 in Wiley InterScience (www.interscience.wiley.com). DOI: 10.1002/fld.1611

SHORT COMMUNICATION

Solution to Euler equations by high-resolution upwind compact scheme based on flux splitting

Hu Jun, Shaogang Guo*,† and Zhenqiang Yao

School of Mechanical and Power Energy Engineering, Shanghai Jiao Tong University, Shanghai 200240, China

SUMMARY

A high-resolution upwind compact method based on flux splitting is developed for solving the compressive Euler equations. The convective flux terms are discretized by using the modified advection upstream splitting method (AUSM). The developed scheme is used to compute the one-dimensional Burgers equation and four different example problems of supersonic compressible flows, respectively. The results show that the high-resolution upwind compact scheme based on modified AUSM+ flux splitting can capture shock wave and other discontinuities, obtain higher resolution and restrain numerical oscillation. Copyright © 2007 John Wiley & Sons, Ltd.

Received 7 December 2006; Revised 29 May 2007; Accepted 21 July 2007

KEY WORDS: Euler equations; compact scheme; convective flux terms

1. INTRODUCTION

In recent years, the compact scheme has been widely used in the large area of computational problems, for example, to compute hyperbolic equations. Generation of compact schemes is considered in [1, 2]. There were also some works on improving the compact scheme directly or on solving two-dimensional incompressible and compressible flow problems with the conventional compact schemes by combining the flux splitting [3, 4]. In this paper, not only the flux-splitting schemes are improved but also a symmetric filtering term is added to the compact schemes to obtain high-resolution upwind compact scheme.

The primary objective of numerical schemes for solving applied gas dynamics problems is to maximize both robustness and accuracy. This requirement is particularly important in Euler solutions in high-speed regimes and complicated boundary layer near wall where intense shock waves

*Correspondence to: Shaogang Guo, School of Mechanical and Power Energy Engineering, Shanghai Jiao Tong University, Shanghai 200240, China.
†E-mail: guoshaogang1217@yahoo.com.cn

and boundary layers may exist simultaneously. High-order compact schemes have had rapid development in recent years due to their narrow grid stencil, enhanced accuracy and better resolution characteristics over the non-compact conventional schemes. Especially Lele [1] has put forward high-order compact schemes based on the Hermite method, which can deal with complicated boundary layer but produce mendacious oscillation in discontinuities. The paper presents a high-resolution upwind compact scheme based on flux splitting which can deal with discontinuities better.

Flux splitting mainly includes flux vector splitting (FVS) and flux difference splitting (FDS). Current trend in the development of upwind schemes focused on the construction of hybrid flux-splitting formulations which seeks to combine FVS with FDS. FVS was put forward by Steger and Warming [5] and Van Leer [6], respectively. This scheme is simple and robust in the capture of intense shocks and rarefaction waves. The high-order compact methods developed by Cockburn and Shu [7], Mawlood *et al.* [8] and Ravichandran [9] among others are successful examples of FVS-based schemes. The drawback of FVS methods is that there exist accuracy problems in resolving shear layer regions due to the excessive numerical dissipation error associated with them.

In contrast, FDS such as Roe's scheme that utilizes the solution of the local Riemann problem usually provides accurate solutions. The numerical methods developed by Deng and Maekawa [10] for solving the Euler equations and Deng and Zhang [11] for solving the Euler and Navier–Stokes equations are examples of high-order compact methods that utilize Roe's FDS. Unfortunately, Roe's scheme has a number of robustness problems such as the violation of entropy condition and the carbuncle phenomenon.

Liou and Steffen [12] put forward the advection upstream splitting method (AUSM), which belongs to upwinded scheme. The most important idea lies in including convection and sound wave influence in the process of flow transmit. It disparts the inviscid flux in the Euler equations: the convective and pressure terms. This scheme develops rapidly and became more mature AUSM+ scheme soon. It has the ability to distinguish physical discontinuities as shock wave, slipstream, etc. and can remain positive. It can deal with the transmit of discontinuities such as shock wave. Especially, the modified AUSM+ splitting approach by Dewang and Wang [13] in 2004 not only decreases the numerical oscillation and improves resolution but also increases the precision and constringency.

In this paper, a high-resolution upwind compact scheme that is based on the modified AUSM+ flux splitting is developed and tested. The effect of gradient of the pressure is introduced to improve the AUSM+ flux splitting scheme, and a symmetric filtering term is added to the compact scheme to obtain a high-resolution upwind scheme. The numerical method is tested in the Burgers equation and in four different example problems about supersonic compressible flows, Sod's problem, interaction of a moving shock with a density wave, double Mach reflection problem and oblique shock reflection problem, respectively. This shows that the present compact scheme based on modified AUSM+ flux splitting can capture shock wave and other discontinuities, obtain high resolution and proper solution and restrain numerical oscillation much better.

2. GOVERNING EQUATIONS

The two-dimensional compressible Governing equations can be written in the conservation form as

$$\frac{\partial Q}{\partial t} + \frac{\partial E}{\partial x} + \frac{\partial F}{\partial y} = 0 \tag{1}$$

DOI: 10.1002/fld

where

$$Q=\begin{bmatrix}\rho\\ \rho u\\ \rho v\\ \rho e\end{bmatrix},\quad E=\begin{bmatrix}\rho u\\ \rho u^2+p\\ \rho uv\\ \rho uH\end{bmatrix},\quad F=\begin{bmatrix}\rho v\\ \rho uv\\ \rho v^2+p\\ \rho vH\end{bmatrix}$$

ρ, r, u, v, p, e and H are the density, the x-component of the velocity, the y-component of the velocity, the pressure, the total energy and the total enthalpy, respectively. The total enthalpy H is related to the other quantities by the following relation:

$$H=e+\frac{p}{\rho}$$

For a perfect gas, the total energy is given by

$$e=\frac{p}{(\gamma-1)\rho}+\frac{1}{2}(u^2+v^2)$$

where γ is the ratio of specific heats and takes the value of 1.4 for air. The normalization has been carried out by using the following free-stream reference: density ρ_∞, sonic speed a_∞, pressure $\rho_\infty c_\infty^2$; the sonic speed is defined as $a=\sqrt{rp/\rho}$.

In fact, a system of coordinates is often transformed based on different flow problems in order to make calculation easier. Equation (1) can be transformed from Cartesian coordinates (x, y) into computed coordinates (ξ, η) as

$$\frac{\partial\widetilde{Q}}{\partial t}+\frac{\partial\widetilde{E}}{\partial\xi}+\frac{\partial\widetilde{F}}{\partial\eta}=0 \tag{2}$$

where

$$\widetilde{Q}=\frac{Q}{J},\quad \widetilde{E}=\frac{(\xi_x E+\xi_y F)}{J},\quad \widetilde{F}=\frac{(\eta_x E+\eta_y F)}{J}$$

here

$$\xi_x=Jy_\eta,\quad \xi_y=-Jx_\eta,\quad \eta_x=-Jy_\xi,\quad \eta_y=Jx_\xi$$

and the Jacobian of the transformation is given by

$$J=\frac{1}{(x_\xi y_\eta-x_\eta y_\xi)}$$

3. SPATIAL DISCRETIZATION

Dewang and Wang [13] have pointed out that conventional AUSM+ scheme leads to numerical oscillation without dealing with the sonic speed, although it does not have 'carbuncle' phenomena. Therefore, in the hybrid modified AUSM+ flux splitting, the sonic speed is expressed as

DOI: 10.1002/fld

$a_{1/2}=\frac{1}{2}(a_L+a_R)$. Because the ε-direction discretization is similar to the η-direction discretization, the present paper introduces only the former discretization. The mid-point numerical flux, using the modified AUSM+ splitting approach, can be expressed as

$$\widetilde{E}_{i+1/2,j}=\frac{M_{1/2}\sqrt{\xi_x^2+\xi_y^2}}{J}(\Psi_L+\Psi_R)-\frac{|M_{1/2}|'\sqrt{\xi_x^2+\xi_y^2}}{J}(\Psi_R-\Psi_L)+\frac{1}{J}(p_\xi^+\theta_L+p_\xi^+\theta_R) \tag{3}$$

Here, the flux function is split into convective section and sound wave section; the first two terms represent convective term, and the last one is the pressure term:

$$\psi=\begin{bmatrix}\rho a\\ \rho u a\\ \rho v a\\ \rho H a\end{bmatrix},\quad \theta=\begin{bmatrix}0\\ \xi_x p\\ \xi_y p\\ 0\end{bmatrix}$$

$M_{1/2}$ is the numerical value of the Mach number:

$$M_{1/2}=(1+\widetilde{E}_L)M_{\xi L}^+ + (1+\widetilde{E}_R)M_{\xi R}^-$$

This method to deal with $M_{1/2}$ can restrain numerical oscillation on the boundary layer near the wall. Here

$$M_\xi^\pm=\begin{cases}\frac{1}{2}(M_\xi\pm|M_\xi|) & |M_\xi|\geqslant 1\\ \pm\frac{1}{4}(M_\xi\pm 1)^2\pm\frac{1}{8}(M_\xi^2-1)^2 & |M_\xi|<1\end{cases}$$

and

$$P_\xi^\pm=\begin{cases}\frac{1}{2}(1\pm\operatorname{sgn}(M_\xi)) & |M_\xi|\geqslant 1\\ \pm\frac{1}{4}(M_\xi\pm 1)^2(2\mp M_\xi)\pm\frac{3}{16}M_\xi(M_\xi^2-1)^2 & |M_\xi|<1\end{cases}$$

$$|M_{1/2}|'=\begin{cases}|M_{1/2}| & |M_{1/2}|\geqslant\delta_0\\ \dfrac{|M_{1/2}|+\delta_0^2}{2\delta_0} & |M_{1/2}|<\delta_0,\quad \delta_0=0.1\cdot|M_\infty|\end{cases}$$

where, taking into account the effect of gradient of pressure, $\widetilde{E}_L$ is expressed as

$$\widetilde{E}_L=\begin{cases}\dfrac{p_{\xi,L}-p_{\xi,R}}{p_{\xi,L}+p_{\xi,R}}\varphi(p_{\xi,L},p_{\xi,R})\cdot|f_{M,L}^\pm|\cdot\min\left[1,\left(\dfrac{|V_{\xi,L}|}{\alpha_{1/2}}\right)^{0.25}\right] & |M_{\xi,L}|<1\\ 0 & |M_{\xi,L}|\geqslant 1\end{cases} \tag{4}$$

Obviously, it is similar to a limiter.

DOI: 10.1002/fld

Here,

$$f^{\pm}_{M,L} = \begin{cases} \frac{1}{2}(M_{\xi,L} \pm |M_{\xi,L}|) & |M_{\xi,L}|>1 \\ \pm \frac{1}{4}(M_{\xi,L} \pm 1)^{1/2} & |M_{\xi,L}|\leqslant 1 \end{cases}$$

$$\varphi(a,b) = \begin{cases} 4\min\left(\frac{a}{b}, \frac{b}{a}\right) - 3 & \min\left(\frac{a}{b}, \frac{b}{a}\right) \geqslant \frac{3}{4} \\ 0 & 0 \leqslant \min\left(\frac{a}{b}, \frac{b}{a}\right) < \frac{3}{4} \end{cases}$$

In [14], every term in (4) was described in detail. $\varphi(p_{\xi,L}, p_{\xi,R})$ makes the function $\widetilde{E}_L$ go to zero in large pressure gradient; $f^{\pm}_{M,L}$ is designed to reduce the order of magnitude of the function $\widetilde{E}_L$, and $\min[1, (|V_{\xi,L}|/\alpha_{1/2})^{0.25}]$ makes the function $\widetilde{E}_L$ vanish in the stagnation region. As for $\min[1, (|V_{\xi,L}|/\alpha_{1/2})^{0.25}]$, it has been stated very detailedly in [14]; hence we are not repeating. $\widetilde{E}_R$ is symmetrical with $\widetilde{E}_L$, and it is not restated here.

The left $(\cdot)$L and right $(\cdot)$R states are obtained by a fourth-order MUSCL polynomial [15]. The high-order approximations to the first-order derivatives are then obtained by the sixth-order central compact scheme of Lele [1], but the discretization of the flux term is a little different; the discretized point is selected in the middle of two grid points; hence, the corresponding coefficient of the discretized point must be changed. The scheme is presented as follows:

$$\begin{aligned} &0.0895(\widetilde{E}'_{i-2,j} + \widetilde{E}'_{i+2,j}) + 0.57967(\widetilde{E}'_{i-1,j} + \widetilde{E}'_{i+1,j}) + \widetilde{E}'_{i,j} \\ &= \frac{1}{\Delta\xi}[1.2988(\widetilde{E}_{i+1/2,j} - \widetilde{E}_{i-1/2,j}) + 0.33539(\widetilde{E}_{i+3/2,j} - \widetilde{E}_{i-3/2,j}) \\ &\quad + 0.006078(\widetilde{E}_{i+5/2,j} - \widetilde{E}_{i-5/2,j})] \end{aligned} \tag{5}$$

In fact, the high-resolution upwind schemes can be formed by adding a symmetric filtering term to the asymmetric explicit part of a central compact schemes: the idea has been interpreted by De and Esmaran [16].

Here, $\widetilde{E}'_{i,j}$ is the higher-order approximation to the first-order derivatives. Equation (5) is used for evaluating the derivatives at the interior points. At the boundaries, the following one-sided compact schemes are used:

$$\widetilde{E}'_{1,j} - \widetilde{E}'_{2,j} = \frac{1}{\Delta\xi}(-\widetilde{E}_{3/2,j} + 2\widetilde{E}_{5/2,j} - \widetilde{E}_{7/2,j}) \tag{6}$$

$$\widetilde{E}'_{i\max,j} - \widetilde{E}'_{i\max-1,j} = \frac{1}{\Delta\xi}(\widetilde{E}_{i\max-1/2,j} - 2\widetilde{E}_{i\max-3/2,j} + \widetilde{E}_{i\max-5/2,j}) \tag{7}$$

Evaluation of the η-direction derivatives is carried out in the same manner and is not shown here.

DOI: 10.1002/fld

4. NUMERICAL RESULTS

In this section calculations are carried out for the Burgers equation and four different examples of compressible flow. Example 1 is the solution of the one-dimensional Burgers equation. Example 2 is Sod's problem. Example 3 is the interaction of a moving shock with a density wave. Example 4 is double Mach reflection problem. Example 5 is the oblique shock reflection problem.

4.1. Example 1: one-dimensional Burgers equation

The steady-state solution of the one-dimensional Burgers equation is solved with a source term

$$u_t + \left(\frac{u^2}{2}\right)_x = \frac{\sin 2x}{2}$$

with the initial condition $u(x, 0) = 2\sin x$ and the boundary condition $u(0, t) = u(\pi, t) = 0$. This problem was studied in [17] as an example of multiple steady-state solutions for characteristic initial value problems. A smooth steady-state solution $u(x, \infty) = \sin x$ is given here. Errors for the one-dimensional Burgers equation are calculated using the present scheme and the AUSM+ scheme, respectively. The numerical results are given in Table I. It is clear that the present scheme can give much less error than the AUSM+ scheme.

4.2. Example 2: Sod's problem and Lax's problem

For Sod's problem, the initial condition is

$$(\rho, u, p)^{\mathrm{T}} = \begin{cases} (0.125, 0, 0.1) & x \geqslant 0.5 \\ (1, 0, 1)^{\mathrm{T}} & x < 0.5 \end{cases}$$

and it uses the computational mesh which is composed of 100 grid point.

Figures 1 and 2 show two computational results of the distributions for the density at $t = 0.18$ by the AUSM+ scheme and the present scheme, respectively, in comparison with the exact solution. Obviously, it can be seen that the upwind compact scheme based on flux splitting has good convergence, and the present scheme has higher accuracy and resolution than the AUSM+ scheme. For the AUSM+ scheme, 3–4 grid points are needed to resolve the shock wave, rarefaction wave and density discontinuity distinctly by AUSM+ scheme, whereas the present scheme needs only 1–2 grid point to distinguish these physical discontinuities clearly.

Table I. Errors of the present scheme and the AUSM+ scheme for the one-dimensional Burgers equation with N cells.

	The present scheme		AUSM+	
N	L^1 error	L^∞ error	L^1 error	L^∞ error
20	5.7647e−04	9.6327e−04	1.3297e−03	7.6970e−03
40	4.1263e−05	7.3726e−05	7.6321e−04	3.4312e−04
80	6.0728e−06	8.9436e−06	8.7143e−05	1.1731e−05
160	8.7326e−08	1.0727e−07	4.3450e−07	2.0041e−06
320	9.3723e−09	2.0314e−08	7.1344e−08	1.4378e−07

DOI: 10.1002/fld

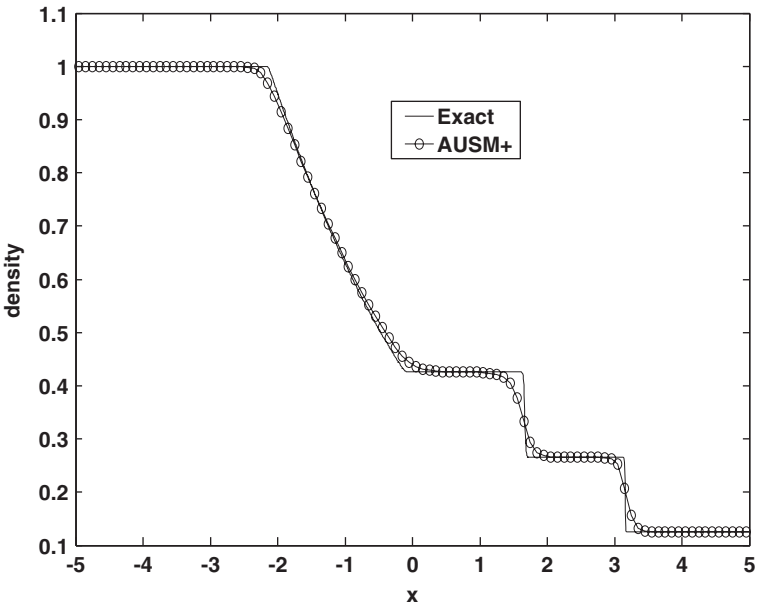

Figure 1. Density distribution (AUSM+).

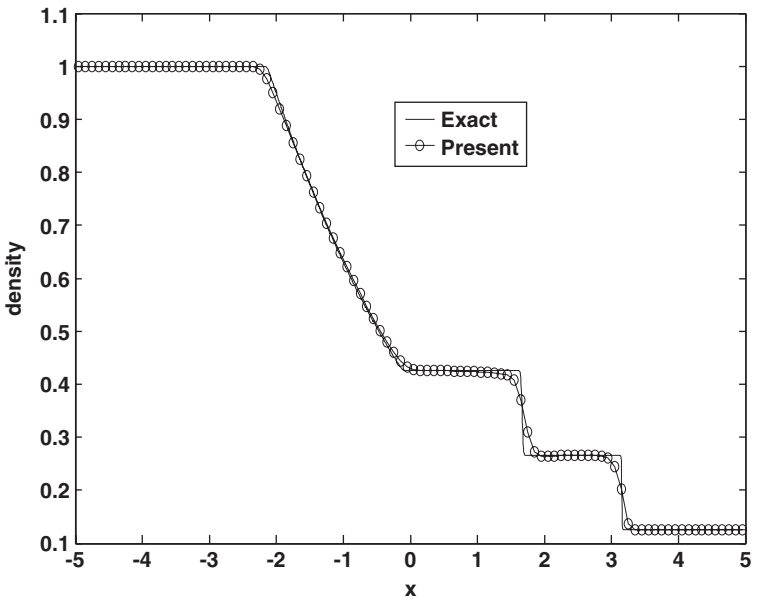

Figure 2. Density distribution (the present scheme).

DOI: 10.1002/fld

4.3. Example 3: interaction of a moving shock with a density wave

The high-resolution upwind compact scheme based on the modified AUSM+ flux splitting scheme is applied to Shu and Osher's one-dimensional shock/turbulence interaction model problem [18] in comparison with AUSM+ scheme. Shock/turbulence interaction problem describes the interaction between a moving Mach 3 shock wave and a fluctuating density sine wave [19]. The initial flow conditions are given by

$$(\rho, u, p)^{\mathrm{T}} = \begin{cases} (1 + 0.2\sin(5x), 0, 1) & x \geqslant 1.0 \\ (3.857143, 2.629369, 10.33333)^{\mathrm{T}} & x < 1.0 \end{cases}$$

The computational domain, $0 \leqslant x \leqslant 10$, is covered with 400 and 200 nodes, respectively. We use the method in [20] to obtain the 'exact' solution, but the number of grid points adds to 4000. It means that the numerical solution of the AUSM+ scheme with 4000 grid points is regarded as the reference data and it is assumed as the exact solution.

The numerical solutions using the present scheme and the AUSM+ scheme are shown in Figures 3 and 4. AUSM+ scheme uses 400 grid points to display the density distribution, whereas the present scheme uses 200 and 400 grid points, respectively. It is clear that the present schemes perform better than AUSM+ schemes, and the former can almost obtain the similar accuracy to the latter with only a half of grid points. This means the upwind compact scheme based on flux splitting plays an important role in decreasing the quantity of calculation. Specifically, AUSM+ schemes produce poorer results in resolving the post-shock entropy waves. The present schemes can capture these waves more correctly with the same grid points.

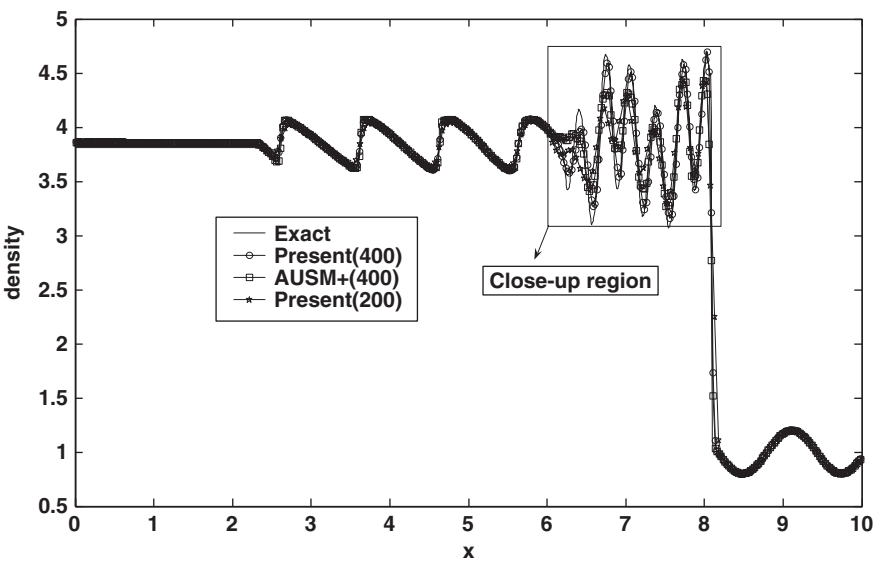

Figure 3. Density distributions of the one-dimensional shock/turbulence interaction.

DOI: 10.1002/fld

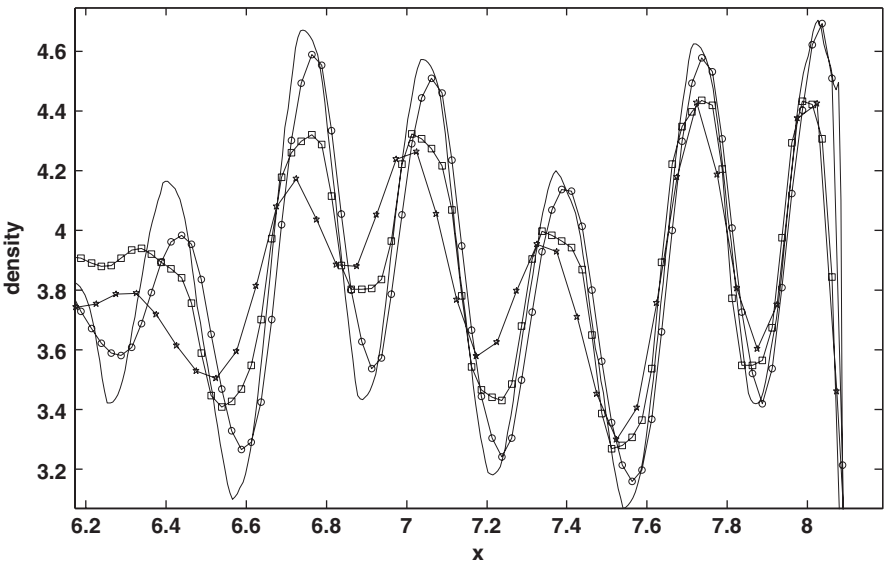

Figure 4. Close-up view of Figure 3.

4.4. Example 4: double Mach reflection problem

This problem was initially proposed and studied in detail by Woodward and Colella [21]. It has been used extensively as a test case in the literature for high-resolution schemes. In this case, a strong shock wave impinges on a ramp with a 30° angle. The inlet flow is a strong shock wave whose Mach number is 10. In order to simplify the problem, the inlet shock wave is inclined with a 60° angle with the axis, and the computational domain is beginning with $x = 1/6$. The computational domain for this problem is chosen to be $(0, 4) \times (0, 1)$. For the top boundary of the computational domain, the solution is set to describe the exact motion of the Mach 10 shock. The left boundary is set as the exact post-shock condition, whereas the right boundary is set as outflow boundary. The initial condition is set:

$$u(x, y, 0) = \begin{cases} u_L, & y \geqslant h(x, 0) \\ u_R, & y < h(x, 0) \end{cases}$$

Here, left and right state values and shock wave's heights are

$$u_L = (8, 57.1597, -33.0012, 563.544), \quad u_L = (8, 57.1597, -33.0012, 563.544)$$

$$h(x, t) = \sqrt{3}\left(x - \frac{1}{6}\right) - 20t$$

and computational grid number is 960×240; the results at $t = 0.2$ are shown. In all the plots, we use 30 contours equally distributed from $\rho = 1.5$ to 22.7.

Figure 5 is the numerical solution of the present scheme, and Figure 6 is calculated using the AUSM+ scheme. Figure 7 is the close-up view of Figures 5 and 6 for the 'blown-up' domain. Note that this detailed structure is of physical interest and was studied before with an adaptive grid

DOI: 10.1002/fld

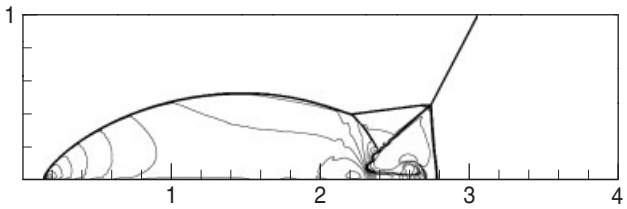

Figure 5. Double Mach reflection problem (the present scheme), $t = 0.2$, density contours (960×240).

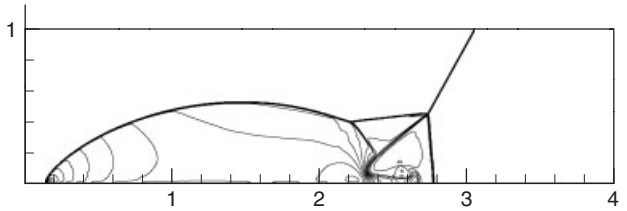

Figure 6. Double Mach reflection problem (AUSM+), $t = 0.2$, density contours (960×240).

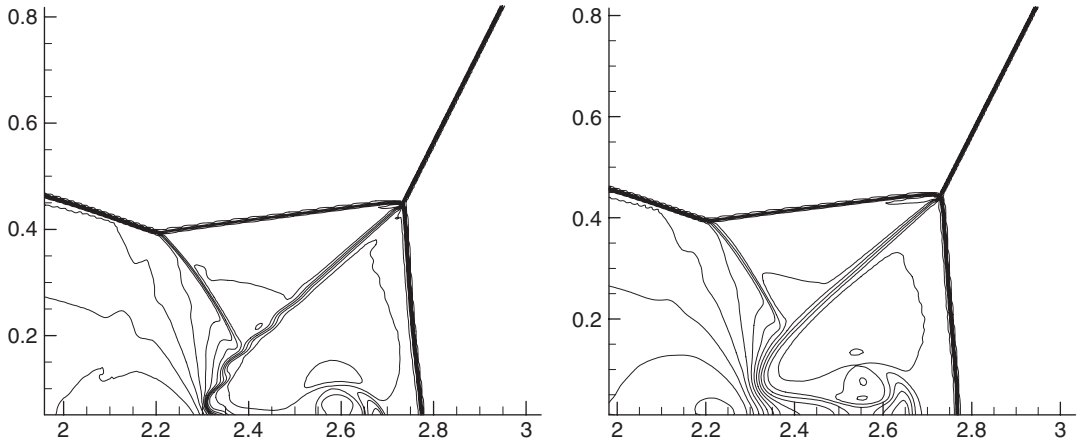

Figure 7. Close-up view of Figures 5 and 6 (around $x = 2$–3).

calculation in [22]. It is not easy to observe any significant difference between the present scheme and the AUSM+ scheme in Figures 5 and 6. However, if we show a 'blown-up' portion around the double Mach region, as shown in Figure 7, it can be seen that the present scheme gives a much better resolution for these structures than the AUSM+ scheme with the same number of elements.

4.5. Example 5: oblique shock reflection problem

The first two-dimensional considered test case is the reflection of a shock wave on an inviscid wall. The shock angle is 33° from the Mach 3 free stream. The mesh size is 60×20 and is uniformly

DOI: 10.1002/fld

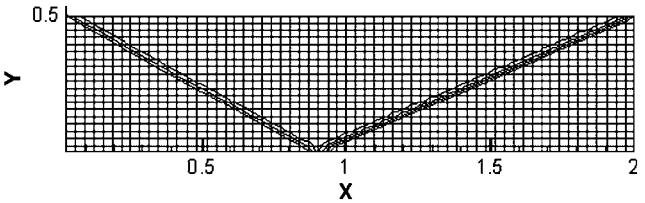

Figure 8. Oblique shock reflection problem, $t = 2.0$, pressure contours.

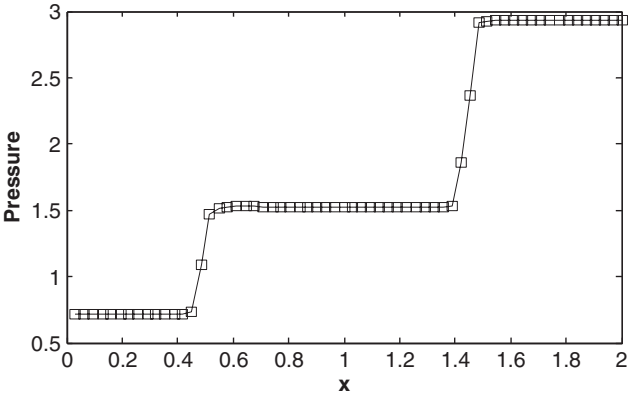

Figure 9. The contribution of pressure in $y = 0.25$.

distributed in both directions. The jump conditions are imposed on the upper boundary, whereas slip wall conditions are set at the bottom boundary. Pressure field is plotted in Figure 8. Figure 9 shows the distributions for the pressure in $y = 0.25$. Although the shock wave is not aligned with the computational mesh, no significant wiggles are presented around the discontinuity which is well captured. The results are in good agreement with the numerical solution presented in [23], but upwind compact scheme based on AUSM+ flux splitting needs fewer cells. Especially the present scheme needs only 1–2 grid points to realize the transition in the discontinuities and this means that the present scheme can obtain acceptable results by using fewer cells.

5. CONCLUSIONS

A high-resolution upwind compact method is developed for solving the Euler equations. The method is based on the modified AUSM+ flux splitting and a high-resolution upwind compact scheme. The numerical results show that the present scheme not only needs less grid numbers as a compact scheme but also has higher resolution in distinguishing physical discontinuities such as shock wave and restrain numerical oscillation. The present scheme is a high-resolution upwind scheme. Especially we modify the AUSM+ scheme considering the subsonic conditions; hence, the scheme can be applied to the solution for different subsonic and supersonic flow.

DOI: 10.1002/fld

REFERENCES

1. Lele SK. Compact finite difference schemes with spectral-like resolution [J]. *Journal of Computational Physics* 1992; **103**(1):16–42.
2. Carey GF, Spotz WF. Higher-order compact mixed methods. *Communications in Numerical Methods in Engineering* 1997; **13**:553–564.
3. Mawlood MK, Basri S. Solution of Navier–Stokes equations by fourth-order compact schemes and AUSM flux splitting. *International Journal of Numerical Methods for Heat and Fluid Flow* 2006; **16**:107–120.
4. Mahesh K. A family of high order finite difference schemes with good spectral resolution. *Journal of Computational Physics* 1998; **145**:332–358.
5. Steger JL, Warning RF. Flux vector splitting of the inviscid gas dynamics equations with application to finite difference methods. *Journal of Computational Physics* 1981; **40**:263–293.
6. Van Leer B. Towards the ultimate conservation difference scheme V.A. second order sequel to Godunov's method. *Journal of Computational Physics* 1979; **32**:101–136.
7. Cockburn B, Shu CW. Nonlinearly stable compact schemes for shock calculation. *SIAM Journal on Numerical Analysis* 1994; **31**:607–627.
8. Mawlood MK, Asrar W, Omar AA, Basri S. A high resolution compact upwind algorithm for inviscid flows. *AIAA-2003-0076*.
9. Ravichandran KS. High order KFVS algorithm using compact upwind difference operators. *Journal of Computational Physics* 1997; **43**:357–372.
10. Deng X, Maekawa H. Compact high-order accurate nonlinear schemes. *Journal of Computational Physics* 1997; **130**:77–91.
11. Deng X, Zhang H. Developing high-order weighted compact nonlinear schemes. *Journal of Computational Physics* 2000; **165**:22–44.
12. Liou MS, Steffen CJ. A new flux splitting scheme. *Journal of Computational Physics* 1993; **107**:23–29.
13. Dewang L, Wang K. The modified AUSM+ scheme. *Acta Aerodynamica Sinica* 2004; **22**(4):404–409.
14. Kim KH, Lee JH, Rho OH. An improvement of AUSM schemes by introducing the pressure-based weight functions [j]. *Computer and Fluids* 1998; **3**(27):311–346.
15. Yamamoto S, Daiguji H. Higher-order-accurate upwind schemes for solving the compressible Euler and Navier–Stokes equations. *Computers and Fluids* 1993; **22**:259–270.
16. De AK, Eswaran V. Analysis of a new high resolution upwind compact scheme. *Journal of Computational Physics* 2006; **218**:398–416.
17. Salas MD, Abarbanel S, Gottlieb D. Multiple steady states for characteristic initial value problems. *Applied Numerical Mathematics* 1986; **2**:193–210.
18. Shu CW, Osher S. Efficient implementation of essentially non-oscillatory shock capturing schemes II. *Journal of Computational Physics* 1989; **83**:32–78.
19. Billet G, Louedin O. Adaptive limiters for improving the accuracy of the MUSCL approach for unsteady flows. *Journal of Computational Physics* 2001; **170**:161–183.
20. Kim D, Kwon JH. A high-order accurate hybrid scheme using a central flux scheme and a WENO scheme for compressible flowfield analysis. *Journal of Computational Physics* 2005; **210**:554–583.
21. Woodward P, Colella P. The numerical simulation of two-dimensional fluid flow with strong shocks. *Journal of Computational Physics* 1984; **54**:115–173. ISSN: 0021-9991.
22. Berger M, Colella A. Local adaptive mesh refinement for shock hydrodynamics. *Journal of Computational Physics* 1989; **82**:64.
23. Visbal MR, Gaitonde DV. Shock capturing using compact-differentiated-bases method. *Forty-third AIAA Aerospace Sciences Meeting and Exhibit*, Reno, Nevada, 2005; AIAA Paper 2005-1265.

DOI: 10.1002/fld